Proceedings of ASME 2013 International Mechanical Engineering Congress & Exposition
IMECE 2013
November 15-21, 2013, San Diego, California, USA

IMECE2013-63144

DRAFT:NUMERICAL MODELLING OF ELECTRODE GEOMETRY EFFECTS IN A 2D SELF-FIELD MPD THRUSTER

Carlos M. Xisto*
Departamento de Engenharia Electromecânica
Universidade da Beira Interior
Covilhã 6201-001
Portugal
Email: xisto@ubi.pt

José C. Páscoa
Paulo J. Oliveira
Departamento de Engenharia Electromecânica
Universidade da Beira Interior
Covilhã 6201-001
Portugal
pascoa@ubi.pt; pjpo@ubi.pt

ABSTRACT

A self-field MPD thruster in its most basic form consists in a central cathode surrounded by a concentric anode. With this coaxial geometric shape is very difficult to use experimental techniques to visualize the plasma parameters. In the following paper we intend to present some preliminary results for a 2D self-field MPD thruster obtained with a new algorithm developed for solving the resistive magnetohydrodynamics (MHD) equations. The numerical method is based on the well known PISO algorithm and make use of AUSM-MHD scheme for flux calculation.

NOMENCLATURE

B Magnetic field vector.
B Magnitude of the magnetic field vector.
E Electric field vector.
e_t Total energy.
F Momentum Thrust.
F_{ELM} Electromagnetic component of Thrust.
F_{Term} Thermal component of Thrust.
g_0 Acceleration of gravity.
Ha Hartmann number.
I_{spec} Specific impulse.
j Electric current density.
k_B Boltzmann constant.
$\dot{m}$ Mass flow rate.
n Particle density.
p Thermodynamic pressure.
q Electron charge.
Re Reynolds number.
T Static temperature.
t Time.
U Velocity vector.
V Voltage drop.
x, y, z Cartesian components.
ρ Density.
ε_0 Permittivity of free space.
η Electric resistivity.
σ Electric conductivity.
μ_0 Permeability of free space.
ϑ_{eff} Thruster efficiency.
γ Adiabatic index.

INTRODUCTION

A self-field MPD thruster in its most basic form consists in a central cathode surrounded by a concentric anode [1]. With this coaxial geometric shape is very difficult to use experimental techniques to visualize the plasma parameters. The use of measuring probes can also be problematic since they will disturb the plasma flow. To overcome such problems Toki et al. [2] developed a multichannel two-dimensional device. With their approach an almost uniform current distribution can be obtained

*Address all correspondence to this author.

along the line of sight, which ensures easier optical accessibility to the discharge region. We know that a 2D configuration do not reflect the features of coaxial devices. Nevertheless, the easier optical accessibility makes it possible to use advanced visualization techniques and relate the flow data with the performance data [3]. The huge amount of data that can be collected within a bi-dimensional system, with this configuration, can also be quite useful for the development and validation of numerical tools that can be applied in 3D or 2D axisymmetric MPD nozzles.

The application of numerical codes in the flow-field analysis of magnetoplasmadynamic (MPD) thrusters allows us to understand relevant parameters that are quite difficult to visualize in experiments. However, computing the complex physic that is associated with this kind of devices is not a trivial task. Some of the earlier models assumed that the plasma flow in MPD nozzles behaves like a single conducting fluid [4, 5]. However, this assumption leads to some ambiguity in the definition of plasma transport coefficients, since these are usually defined in a different way for electrons and heavy species [6]. Another approach is to consider the plasma as a single fluid but with different temperatures for heavy species and electrons [7–10]. With this last approach it is possible to compatibilize the simplicity of the single fluid approach and, at the same time, calculate the two distinct transport coefficients in a more realistic way. Nevertheless, a single fluid approach can still be useful for a better understanding of the main acceleration mechanisms that are generated by this kind of systems [11].

In the following paper we intend to present some preliminary results for a self-field MPD thruster. These were obtained with a new algorithm developed for the single fluid resistive magnetohydrodynamics (MHD) equations. This new algorithm is based on an all Mach version of PISO method [12], that was extended and validated for ideal MHD flows by Xisto et al. [13,14].

In the next section we will present the governing equations and in section 3 the numerical method is briefly summarized. In section 4 some validation cases are addressed, we start with the Hunt flow problem were we intend to validate our method for low speed resistive MHD. Regarding ideal MHD validation, two bi-dimensional standard problems are addressed, namely the high density cloud shock wave interaction and the MHD rotor. Finally, in section 5 the effects of cathode geometry in a 2D self-field MPD thruster performance will be analysed.

GOVERNING EQUATIONS

Magnetohydrodynamics is related to the interaction of a conducting moving fluid with one or more magnetic fields. This interaction can be described by the MHD equations, which couple the magnetic field, given by Maxwell equations, with the flow of a conducting fluid, ruled by the Navier-Stokes equations. The resistive form of the MHD system of equations is given by:

$$\frac{\partial \rho}{\partial t} + \nabla \cdot (\rho \mathbf{U}) = 0, \quad (1)$$

$$\frac{\partial \rho \mathbf{U}}{\partial t} + \nabla \cdot \left[\rho \mathbf{U}\mathbf{U} + \left(p + \frac{B^2}{2\mu_0} \right) \mathbf{I} - \frac{\mathbf{B}\mathbf{B}}{\mu_0} - \tau_{visc} \right] = 0, \quad (2)$$

$$\frac{\partial \rho e_t}{\partial t} + \nabla \cdot \left[\left(\rho e_t + p + \frac{B^2}{2\mu_0} \right) \mathbf{U} - \mathbf{U} \cdot \frac{\mathbf{B}\mathbf{B}}{\mu_0} \right] - \nabla \cdot (k \nabla T) - \nabla \cdot \left(\frac{\mathbf{B} \times \eta \mathbf{j}}{\mu_0} \right) = 0, \quad (3)$$

$$\frac{\partial \mathbf{B}}{\partial t} + \nabla \cdot (\mathbf{U}\mathbf{B} - \mathbf{B}\mathbf{U}) + \nabla \times (\eta \mathbf{j}) = 0, \quad (4)$$

where k is the plasma thermal conductivity, $\eta = 1/\sigma$ represents the plasma electric resistivity and μ_0 is the permeability of free space. This system expresses the conservation of mass Eqn. (1), momentum (2), total energy (3), and propagation of the magnetic field (4). The viscous stress tensor for compressible flow is given by:

$$\tau_{visc} = -\left(\frac{2}{3} \mu \nabla \cdot \mathbf{U} \right) \mathbf{I} + \mu \left[\nabla \mathbf{U} + (\nabla \mathbf{U})^T \right], \quad (5)$$

where μ is the dynamic viscosity of the plasma. Temperature is a derived quantity and can be obtained from an equation of state,

$$T = \frac{1}{c_v} \left[e_t - \frac{1}{2} \left(U^2 + \frac{B^2}{\rho \mu_0} \right) \right]. \quad (6)$$

Using Ampère's law, and some vector identities, the last term of Eqn. (4) can be rewritten in terms of **B**:

$$\nabla \times (\eta \mathbf{j}) = \nabla \times \left(\eta \frac{\nabla \times \mathbf{B}}{\mu_0} \right) = -\nabla \cdot \left(\eta \nabla \frac{\mathbf{B}}{\mu_0} \right). \quad (7)$$

The electrical conductivity is treated as a scalar field given by the Spitzer-Harm formulation,

$$\sigma = 1,53 \times 10^{-2} \frac{T^{3/2}}{\ln \Lambda}, \quad (8)$$

where,

$$\ln \Lambda = \ln \left(\frac{12\sqrt{2}\pi \left(k_B \varepsilon_0 T \right)^{3/2}}{q^3 n^{1/2}} \right), \quad (9)$$

is the Coulomb logarithm. In Eqn. (9) k_B is the Boltzmann constant, q is related to electron particle charge, ε_0 is the permittivity of free space and n is the particle density expressed in particles per cubic meter of plasma.

NUMERICAL MODEL

The numerical method that was used for the MPD thruster analysis was developed and validated, for the ideal MHD equations, by Xisto et al. [13, 14]. This new algorithm is based on the PISO method previously developed for the Euler equations and validated for all Mach number flows [12]. In order to improve accuracy and stability in the calculation of all kinds of MHD discontinuities we have adapted the AUSM-MHD scheme proposed by Han et al. [15] and for variable interpolation the CUBISTA limiter was used [16]. For multidimensional MHD cases, in order to ensure $\nabla \cdot \mathbf{B} = 0$, we make use of the hyperbolic diverge cleaning technique proposed by Dedner et al. [17].

Thruster parameters

Several parameters can be used to assess the performance of an MPD thruster. The overall thrust force can be calculated from the momentum flux at thruster exit,

$$F = \int_{out} \left(\rho U^2 + p\right) dS. \tag{10}$$

The electromagnetic component of the total force can be calculated with the volume integral of the axial component of the Lorentz force,

$$F_{ELM} = \int_V (\mathbf{j} \times \mathbf{B})_x \, dV. \tag{11}$$

The thermal contribution can be easily calculated as the difference between total and ELM forces,

$$F_{Term} = F - F_{ELM}. \tag{12}$$

The thruster specific impulse can be calculated in the following way:

$$I_{spec} = \frac{F}{\dot{m} g_0}, \tag{13}$$

where $g_0 = 9{,}8 \left[\mathrm{m/s^2}\right]$ represents acceleration due to gravity. From Eqn. (13) we can conclude that a system that is able to produce an higher specific impulse is more efficient, since it can generate more thrust for the same mass of gas propellant. The efficiency of a self-field bi-dimensional MPD thruster can be calculated in the following way [18].

$$\vartheta_{eff} = \frac{F^2}{2\dot{m} I \left(V + V_{elet}\right)}, \tag{14}$$

where $\dot{m}$ is the mass flow rate and I is the discharge current. The electrical voltage across the plasma, V , that can be calculated as the line integral of Ohm's law from anode to cathode,

$$V = \int \mathbf{E} \cdot dl = \int (\eta \mathbf{j} - \mathbf{U} \times \mathbf{B}) \cdot dl. \tag{15}$$

The numerical model is not able to predict the potential drop due to electric sheath formation near the electrode walls. For that reason a constant value of $V_{elet} = 20\,\mathrm{V}$ was specified [18, 19].

VALIDATION

Regarding validation three test cases will be addressed. We start with the well known Hunt flow problem, were we intend to validate our model for low speed resistive MHD flow. The two remaining cases are standard 2D ideal MHD problems that will be use to validate our model for complex MHD shock interaction.

Resistive MHD validation

The Hunt flow problem is a well know test case for incompressible and resistive MHD flow. This case allows us to validate the effect of the Lorentz force ($\mathbf{j} \times \mathbf{B}$) in the evolution of a conducting fluid in a square duct. The channel is composed by two electrical insulated walls, that are parallel to the applied magnetic field (in this case B_z), and two conducting walls that are perpendicular to the applied field. We consider a fully developed flow with a Reynolds number equal to $Re = 10$ and a Hartmann number equal to $Ha = 300$. The flow is unidirectional (x direction) and is driven by a pressure gradient of $-300\,[\mathrm{Pa/m}]$. For the conducting walls an electrical conductance ratio equal to 0.1 is specified. An analytical solution can be obtained with the hyperbolic functions that were proposed by Hunt [20], or by the exponential version of those equations [21]. The solution was calculated in a 2D non-uniform mesh with 46×46 nodes, see Fig. 1. This problem can be easily converted in a two dimensional case if we only consider one cross-section of the channel with periodic boundary conditions in the flow direction.

In Fig. 2 we present a comparison between analytical and numerical results. We can see that, for both boundary layers, the numerical results tend to agree very well with the analytical solutions. The two side-wall jets are related to the balance between the pressure gradient and the Lorentz force. In the insulated sidewalls the current lines are parallel to the applied magnetic field, thus, the electromagnetic braking force in these regions is significantly reduced. As a consequence, in that region the pressure gradient is mainly balanced by the viscous force and the flow protrudes through the magnetic field in thin jets along the sidewalls [22].

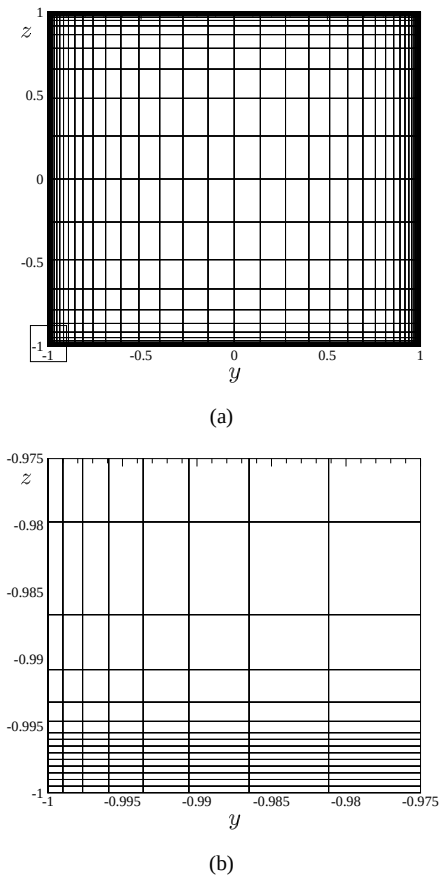

FIGURE 1. NUMERICAL GRID USED FOR THE HUNT FLOW PROBLEM CALCULTION.

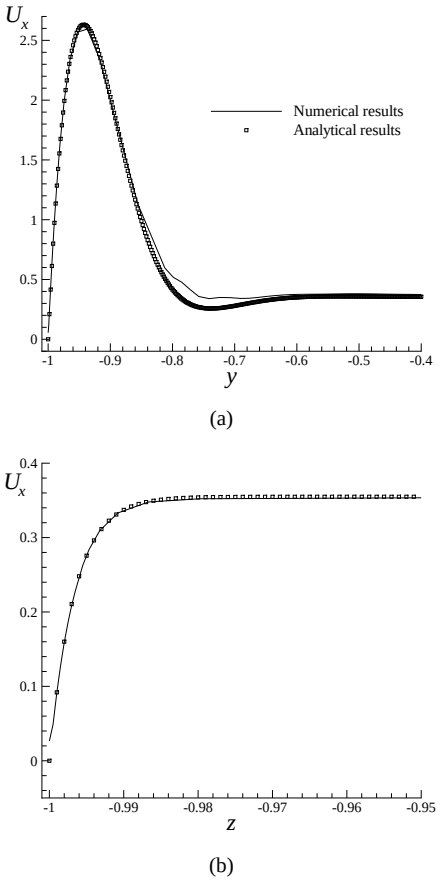

FIGURE 2. COMPARISON BETWEEN NUMERICAL AN ANALYTICAL RESULTS.

Ideal MHD validation

In this section we will address two standard ideal MHD problems. The first test case is related to a well know problem in astrophysics, see citeDai1998a. It comprises the interaction of an high density cloud with a strong shock wave. The computational domain is a square box with $x,y \in [0;1]$ and a total of 400×400 nodes. The discontinuity lies at $x = 0.6$ with the following left and right states for the dependent variables:

$$\begin{pmatrix} \rho[\mathrm{kg/m^3}] \\ U_x[\mathrm{m/s}] \\ U_y[\mathrm{m/s}] \\ U_z[\mathrm{m/s}] \\ p[\mathrm{Pa}] \\ B_x[\mathrm{T}/\mu_0] \\ B_y[\mathrm{T}/\mu_0] \\ B_z[\mathrm{T}/\mu_0] \end{pmatrix} = \begin{pmatrix} 3,86859 \\ 0 \\ 0 \\ 0 \\ 167.345 \\ 0 \\ 2.1826182 \\ -2.1826182 \end{pmatrix}_L = \begin{pmatrix} 1 \\ -11.2536 \\ 0 \\ 0 \\ 1 \\ 0 \\ 0.56418958 \\ 0.56418958 \end{pmatrix}_R , \quad (16)$$

the adiabatic index is equal to $\gamma = 5/3$. The high density cloud ($\rho = 10[\mathrm{kg/m^3}]$) assumes a circular shape with centre in $(x,y) \in (0.8;0.5)$ and radius equal to $0.15[\mathrm{m}]$. The value of pressure inside and outside the circular cloud is $p = 1[\mathrm{Pa}]$, so the cloud is in hydrostatic equilibrium with the environment. Regarding boundary conditions, in the right there is a fixed value boundary condition due to supersonic flow, and in the remaining boundaries the variables are extrapolated from inside the domain.

The results were obtained for a final time of $t = 0.06\,[\mathrm{s}]$, before the cloud leave the domain. In Fig. 3 a) we present the contour plots for density in a logarithmic colour scale and in Fig. 3 b) the magnetic field lines are plotted. We can observe that the discontinuities are calculated with a good resolution. This case does not have any analytical solution, and it can only be compared with solutions from different authors, see [23,24]. The second test case comprises the so called MHD rotor. This case can be found in [25] and it allows us to test our model for the calculation of torsional Alfvén waves. The rotation speed is an initial condition of the problem an no other external forces are

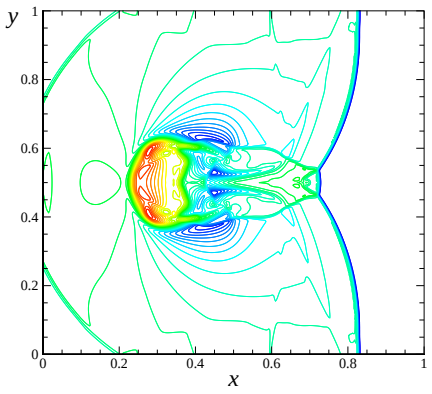

(a)

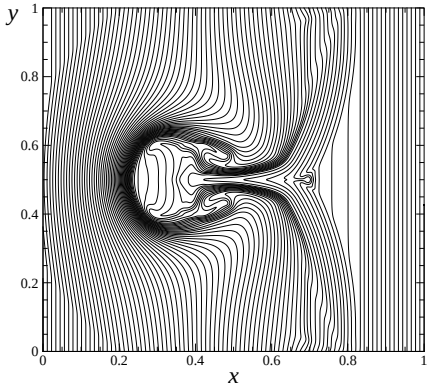

(b)

FIGURE 3. NUMERICAL RESULTS OBTAINED FOR THE CLOUD-SHOCK INTERACTION.

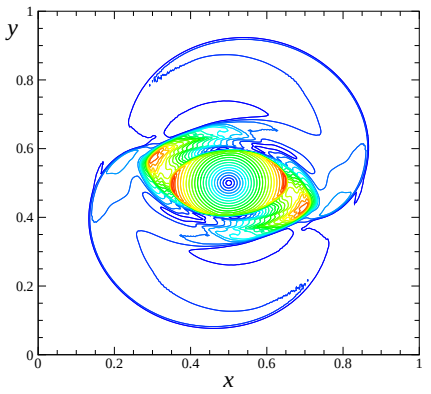

(a)

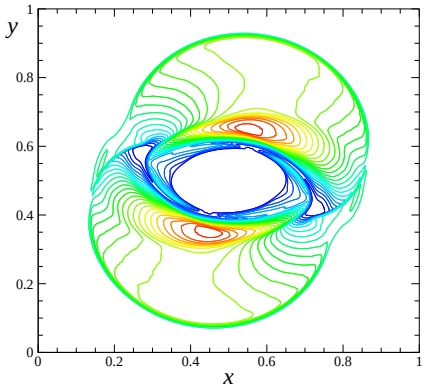

(b)

FIGURE 4. RESULTS OBTAINED FOR THE MHD ROTOR.

applied to the rotor. This problem is again solved in a square domain $x,y \in [0;1]$ with a total of 400×400 nodes. The initial conditions for the magnetic field and pressure are uniform,

$$B_y = 0\,[\mathrm{T}/\mu_0];\; B_x = 5/\sqrt{4\pi}\,[\mathrm{T}/\mu_0];\; p = 1\,[\mathrm{Pa}];\; \gamma = 1.4. \quad (17)$$

The initial conditions for the rotating cylinder of radius $r_0 = 0.1\,[\mathrm{m}]$ are the following:

$$\rho = 10\,[\mathrm{kg/m^3}];\; U_x = -U_0\frac{(y-0,5)}{r_0};\; U_y = U_0\frac{(x-0,5)}{r_0}. \quad (18)$$

Notice that U_x and U_y are functions of $r < r_0$, where $r = \left[(x-0,5)^2 - (y-0,5)^2\right]^{1/2}$ and $U_0 = 2\,[\mathrm{m/s}]$. The environment is defined by the region $r > r_1$ ($r_1 = 0.115\,[\mathrm{m}]$) and its stationary ($U_x = U_y = 0\,[\mathrm{m/s}]$) with a density ten times lower than the cylinder ($\rho = 1\,[\mathrm{kg/m^3}]$). In order to obtain a soft transition between the rotating cylinder and the environmental fluid another region was created, with linear profiles for density and velocity,

$$\rho = 1 + 9f;\; U_x = -fU_0\frac{(y-0,5)}{r};\; U_y = fU_0\frac{(x-0,5)}{r}; \quad (19)$$

where,

$$f = (r_1 - r)\,/\,(r_1 - r_0)\,. \quad (20)$$

In Fig. 4 we present the results obtained after $t = 0.15[\mathrm{s}]$, before the torsional waves reach the computational domain boundary. We can see from the Mach number distribution (Fig. 4a) that the rotor is still rotating, to a certain radial distance, with an uniform angular velocity. Beyond that distance the the rotational speed decreases because the rotor exchange angular momentum with the environment. We can see that the proposed method can calculate torsional Alfvén waves, those waves are particularly visible in the plot of magnetic pressure ($\mathbf{B}\cdot\mathbf{B}/2$), Fig. 4 b).

NUMERICAL MODELING OF A 2D MPD THRUSTER

The previously validated model will now be used to analyse a 2D MPD self-field thruster. In following section the effects of cathode size in the MPD performance will be analysed. This kind of study has been done in an experimental level [26, 27] and several numerical studies were also performed [5, 7, 11, 19]. We will demonstrate that the geometric characteristics of the cathode can influence the discharge current pattern which can result in an increase of the electro-thermal component of thrust.

Regarding the numerical model several assumptions were made. The propellent gas is argon and we assume that it is injected in the discharge chamber in a state of total ionization. We can then assume that the plasma can be treated as a single fluid, quasi-neutral in a state of thermal equilibrium ($T = T_e = T_i$). Several phenomena are neglected, namely: viscosity; thermal conductivity; electrical sheath; Hall effect; and radiation processes. Electrical resistivity is given by Spitzer-Harm's formulation, see Eqn. (8). Also, the plasma flow is purely bi-dimensional in the *xy* plane.

For validation purposes we have use the same boundary conditions as [5]. At inlet, because of its subsonic regime, a mass flow rate of $2.5\,\mathrm{g/s}$ is imposed and a temperature of $T = 5000\,\mathrm{K}$ is fixed. Since the flow is supersonic at outlet, all variables are extrapolated from inside the solution domain. In the electrode walls a slip condition is imposed for velocity and a perfectly electrical conducting wall is specified for the magnetic field. For both the insulated wall and symmetric boundary the magnetic field is fixed to zero. At inlet the magnetic field can be calculated as a function of the discharge current,

$$B_0 = \frac{\mu_0 I}{2W}, \tag{21}$$

where I is the discharge current and W represents the width of the thruster, in this case $W = 84\,[\mathrm{mm}]$.

In Fig. 5 the two analysed configurations are presented. Both geometries are composed by flared anodes (FA), where the only difference between the two devices is related to their cathode length. The first configuration, that we refer as FASC, is composed by a short cathode with a length equal to $13\,[\mathrm{mm}]$, the second geometry (FALC) is composed by a long cathode with $40\,[\mathrm{mm}]$ length.

The proposed method was validated against experimental [3] and numerical results from different authors [5, 11]. In Fig. 6 a) the axial velocity distribution along section $y = 0.009\,[\mathrm{m}]$, for a discharge current of $I = 8000\,[\mathrm{A}]$, is compared with the numerical results obtained for the FASC configuration by two different authors. We can see that the calculated velocity is slightly lower but the plot is showing the same pattern. A more accurate validation requires a comparison with experiments. For that purpose, in Fig. 6 b), the numerical results obtained for the momentum thrust

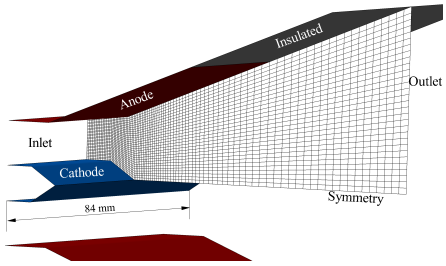

(a)

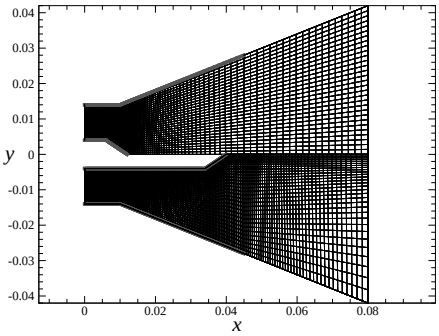

(b)

FIGURE 5. 2D SELF-FIELD MPD THRUSTER GEOMETRY AND BOUDARY CONDITIONS.

in the FASC configuration are compared with experiments. We can see that the current model over-predicts the propulsion force. Nevertheless, the trend is quite similar and when the solution is compared with the results obtained by others [11], while using a similar numerical model, we can observe that our results agree very well.

Lets know analyse the effects of the cathode length for the several thruster parameters. In Fig. 7 a) we compared the overall thrust values obtained with both configurations for several values of discharge current. We can see that with the short cathode configuration we can reach higher values of thrust. This is a related to the geometric shape of the cathode, that will allow a bigger concentration of discharge current lines in is tip, see Fig. 8 a). This feature will increase the thermal component of thrust. In Fig. 7 b) we can see that the ELM component of thrust is almost the same for both devices, and the biggest discrepancy appears in the thermal component of thrust. The results for thruster efficiency and specific impulse are presented in Fig. 9. The configuration FASC can achieve a biggest efficiency for the calculated range of discharge current. This was expected since, for the same mass flow rate and discharge current, this is the configuration that results in higher value of thrust.

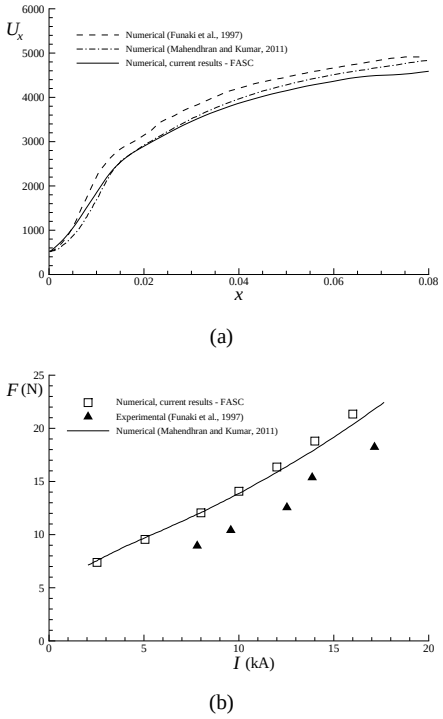

FIGURE 6. COMPARISON BETWENN EXPERIMENTAL AND NUMERICAL RESULTS.

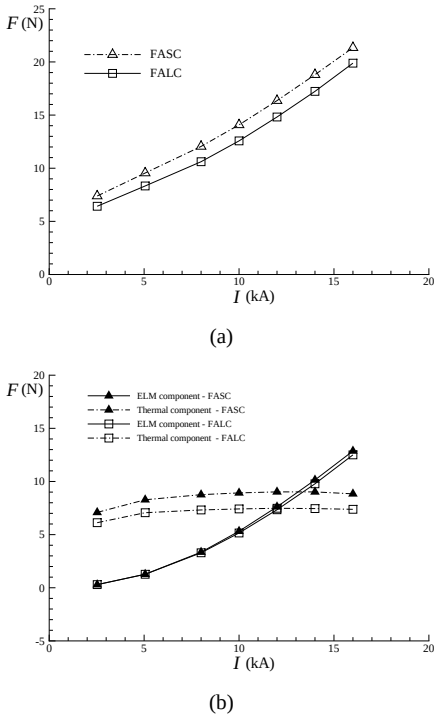

FIGURE 7. RESULTS OBTAINED FOR THRUST IN BOTH CONFIGURATIONS.

CONCLUSIONS

A previously proposed method for the ideal MHD equations was here extended to calculate viscous and resistive MHD flow. The numerical model was validated for resistive MHD using the analytical Hunt flow problem.

Regarding the MPD thruster modelling, a validation against experimental results for a 2D self-field nozzle was also performed. The proposed model over-predicts the values of thrust. However assuming a state of total ionization and thermal equilibrium, while using an ideal gas law, can result in a huge increase of temperature, that will result in a higher thermal component of thrust.

The MPD electrode geometric effects in the thruster performance were also analysed. We have demonstrated that enhancing the electro-thermal component of thrust will result in higher overall thrust values. In a self-field MPD thruster this is achievable by reducing the cathode length.

ACKNOWLEDGMENT

This work was supported by FCT grant SFRH/BD/60285/2009 and by FCT project PTDC/ CTESPA/114163/2009 "SpaceProp - MHD Numerical Modeling in nozzles of MPD Thrusters for Space Propulsion". Additional financial support was provided by CAST.

REFERENCES

[1] LaPointe, M. R., and Mikellides, P. G., 2001. "High power mpd thruster development at the nasa glenn research center". In 37th Joint Propulsion Conference and Exhibit, no. AIAA-2001-3499.

[2] Toki, K., Sumida, M., and Kuriki, K., 1992. "Multichannel two-dimensional magnetoplasmadynamic arcjet". *Journal of Propulsion and Power,* ***8***, pp. 93–97.

[3] Funaki, I., Toki, K., and Kuriki, K., 1998. "Electrode configuration effect on the performance of a two-dimensional magnetoplasmadynamic arcjet". *Journal of Propulsion and Power,* ***14***(6), Nov., pp. 1043–1048.

[4] Sleziona, P., Auweter-Kurtz, M., and Schrade, H., 1988. "Numerical codes for cylindrical mpd trhusters". In Proc. 20th International Electric Propulsion Physics Conference, no. IEPS-88-043.

[5] Funaki, I., Toki, K., and Kuriki, K., 1997. "Numerical analysis of a two-dimensional magnetoplasmadynamic arcjet". *Journal of propulsion and power,* ***13***(6), pp. 789–795.

[6] Myers, R. M., Mantenieks, M. A., and Lapointe, M. R., 1991. Mpd thruster technology. Tech. Rep. NASA-TM-

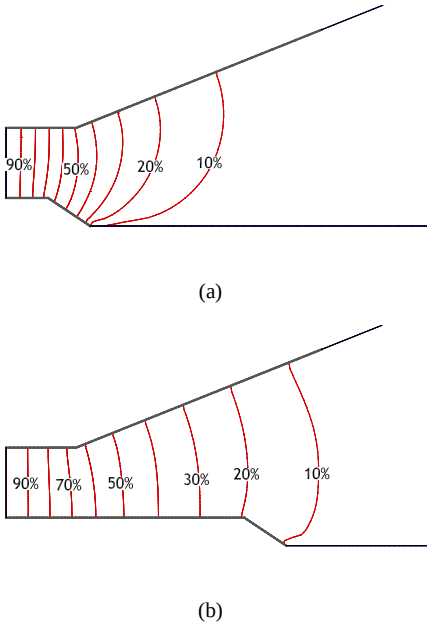

FIGURE 8. MAGNETIC FIELD DISTRIBUTION FOR BOTH CONFIGURATIONS.

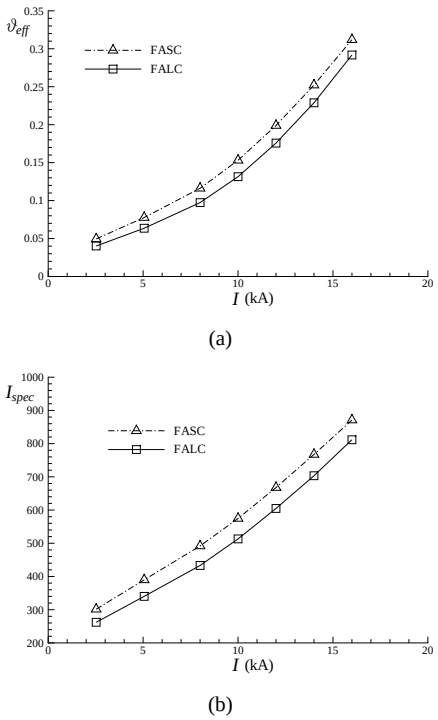

FIGURE 9. EFFICIENCY AND SPECIFIC IMPULSE RESULTS FOR BOTH CONFIGURATIONS.

105242, NASA Glenn Research Center.

[7] LaPointe, M. R., 1992. Numerical simulation of geometric scale effects in cylindrical self-field mpd thrusters. Tech. Rep. CR-189224, NASA Lewis Research Centre.

[8] Sleziona, P. C., Auweter-Kurtz, M., and Schrade, H. O., 1993. "Numerical calculation of a cylindrical mpd thruster". In Procedings 23 International Electric Propulsion Conference, no. IEPC-93-066.

[9] Miyasaka, T., and Fujiwara, T., 1999. "Numerical prediction of onset phenomenon in a 2-dimensional axisymmetric mpd thruster". In *Joint Propulsion Conferences*. American Institute of Aeronautics and Astronautics, June, pp. –.

[10] Sankaran, K., Martinelli, L., Jardin, S. C., and Choueiri, E. Y., 2002. "A flux-limited numerical method for solving the mhd equations to simulate propulsive plasma flows". *International Journal for Numerical Methods in Engineering*, ***53***(6), pp. 1415–1432.

[11] Mahendhran, M., and Kumar, A., 2011. "Numerical study on the effect of electrode geometry in mpd thrusters". In 32nd International Electric Propulsion Conference, no. IEPC-2011-228.

[12] Xisto, C. M., Páscoa, J. C., Oliveira, P. J., and Nicolini, D. A., 2012. "A hybrid pressure density-based algorithm for the euler equations at all mach number regimes". *International Journal for Numerical Methods in Fluids*, ***70:8***, pp. 961–976.

[13] Xisto, C. M., Páscoa, J. C., and Oliveira, P. J., 2012. "Preliminary assessment of a new algorithm for the mhd equations at all mach number regimes". In European Congress on Computational Methods in Applied Sciences and Engineering, ECCOMAS 2012, no. 3212.

[14] Xisto, C., Páscoa, J., and Oliveira, P., 2013. "A pressure-based method with ausm-type fluxes for mhd flows at arbitrary mach numbers". *International Journal for Numerical Methods in Fluids*, pp. n/a–n/a.

[15] Han, S., Lee, J., and Kim, K., 2009. "Accurate and robust pressure weight advection upstream splitting method for magnetohydrodynamics equations". *AIAA Journal*, ***47***, Apr., pp. 970–981.

[16] Alves, M. A., Oliveira, P. J., and Pinho, F. T., 2003. "A convergent and universally bounded interpolation scheme for the treatment of advection". *International Journal for Numerical Methods in Fluids*, ***41***(1), pp. 47–75.

[17] Dedner, A., Kemm, F., Kröner, D., Munz, C.-D., Schnitzer, T., and Wesenberg, M., 2002. "Hyperbolic divergence cleaning for the mhd equations". *Journal of Computational Physics*, ***175***, Jan., pp. 645–673.

[18] Kubota, K., Funaki, I., and Okuno, Y., 2009. "Comparison of simulated plasma flow field in a two-dimensional magnetoplasmadynamic thruster with experimental data". *Plasma Science, IEEE Transactions on*, ***37***(12), pp. 2390–2398.

[19] Kubota, K., Funaki, I., and Okuno, Y., 2007. "Numerical study of electrode geometry effects on flowfield in two-dimensional mpd thrusters". In 30th International Electric Propulsion Conference, no. IEPC-07-87.

[20] Hunt, J. C. R., 1965. "Magnetohydrodynamic flow in rectangular ducts". *Journal of Fluid Mechanics,* ***21***(04), pp. 577–590.

[21] Ni, M.-J., Munipalli, R., Huang, P., Morley, N. B., and Abdou, M. A., 2007. "A current density conservative scheme for incompressible mhd flows at a low magnetic reynolds number. part ii: On an arbitrary collocated mesh". *Journal of Computational Physics,* ***227***(1), pp. 205 – 228.

[22] PRIEDE, J., ALEKSANDROVA, S., and MOLOKOV, S., 2010. "Linear stability of hunt's flow". *Journal of Fluid Mechanics,* ***649***, 3, pp. 115–134.

[23] Dai, W., and Woodward, P. R., 1998. "A simple finite difference scheme for multidimensional magnetohydrodynamical equations". *Journal of Computational Physics,* ***142***(2), pp. 331 – 369.

[24] Tóth, G., 2000. "The $\nabla \cdot \mathbf{B} = 0$ constraint in shock-capturing magnetohydrodynamics codes". *Journal of Computational Physics,* ***161***, July, pp. 605–652.

[25] Balsara, D. S., and Spicer, D. S., 1999. "A staggered mesh algorithm using high order godunov fluxes to ensure solenoidal magnetic fields in magnetohydrodynamic simulations". *Journal of Computational Physics,* ***149***(2), Mar., pp. 270–292.

[26] Funaki, I., Kuriki, K., and Toki, K., 1998. "Electrode configuration effect on the performance of a two-dimensional magnetoplasmadynamic arcjet". *Journal of Propulsion and Power,* ***14***(6), pp. 1043–1048.

[27] Nakata, D., Toki, K., Funaki, I., Shimizu, Y., Kuninaka, H., and Arakawa, Y., 2005. "Experimental verification for the nozzle shape optimization of the self-field mpd thruster". In 29th International Electric Propulsion Conference, no. IEPC-05-163.